Available online at www.sciencedirect.com
ScienceDirect
International Journal of Multiphase Flow 33 (2007) 1074–1087
International Journal of Multiphase Flow
www.elsevier.com/locate/ijmulflow

An experimental study of the regimes of motion of spheres falling or ascending freely in a Newtonian fluid

C.H.J. Veldhuis [a,b], A. Biesheuvel [a,c,*]

[a] J.M. Burgers Centre for Fluid Mechanics, The Netherlands
[b] Physics of Fluids, Department of Applied Physics, Langezijds, University of Twente, P.O. Box 217, 7500AE Enschede, The Netherlands
[c] Engineering Fluid Dynamics, Department of Mechanical Engineering, Horst, University of Twente, P.O. Box 217, 7500AE Enschede, The Netherlands

Received 26 October 2006; received in revised form 7 March 2007

Abstract

This paper presents the results of an experimental investigation aimed at verifying some of the interesting conclusions of the numerical study by Jenny et al. concerning the instability and the transition of the motion of solid spheres falling or ascending freely in a Newtonian fluid. The phenomenon is governed by two dimensionsless parameters: the Galileo number G, and the ratio of the density of the spheres to that of the surrounding fluid ρ_s/ρ. Jenny et al. showed that the $(G, \rho_s/\rho)$ parameter space may be divided into regions with distinct features of the trajectories followed eventually by the spheres after their release from rest. The characteristics of these 'regimes of motion' as described by Jenny et al., agree well with what was observed in our experiments. However, flow visualizations of the wakes of the spheres using a Schlieren optics technique raise doubts about another conclusion of Jenny et al., namely the absence of a bifid wake structure.

PACS: 47.6l.Jd; 47.20.Ky; 47.80.Jk

Keywords: Sphere motion; Path instabilities; Newtonian fluids; Wake structures

1. Introduction

Detailed numerical investigations (Kim and Pearlstein, 1990; Natarajan and Acrivos, 1993; Johnson and Patel, 1999; Ghidersa and Dušek, 2000; Lee, 2000; Tomboulides and Orzag, 2000) have revealed the various wake structures that may be found behind a solid sphere held fixed in a uniform flow, and have unraveled the mechanisms by which these flows become unstable. Experiments by Ormières and Provansal (1999) and Schouveiler and Provansal (2002) have confirmed many of the conclusions of these numerical studies (cf. Fig. 1). The wake is axially symmetric up to a Reynolds number of 212; above this value, a planar-symmetric wake is

* Corresponding author. Address: Engineering Fluid Dynamics, Department of Mechanical Engineering, Horst, University of Twente, P.O. Box 217, 7500AE Enschede, The Netherlands.
E-mail address: a.biesheuvel@utwente.nl (A. Biesheuvel).

0301-9322/$ - see front matter
doi:10.1016/j.ijmultiphaseflow.2007.05.002

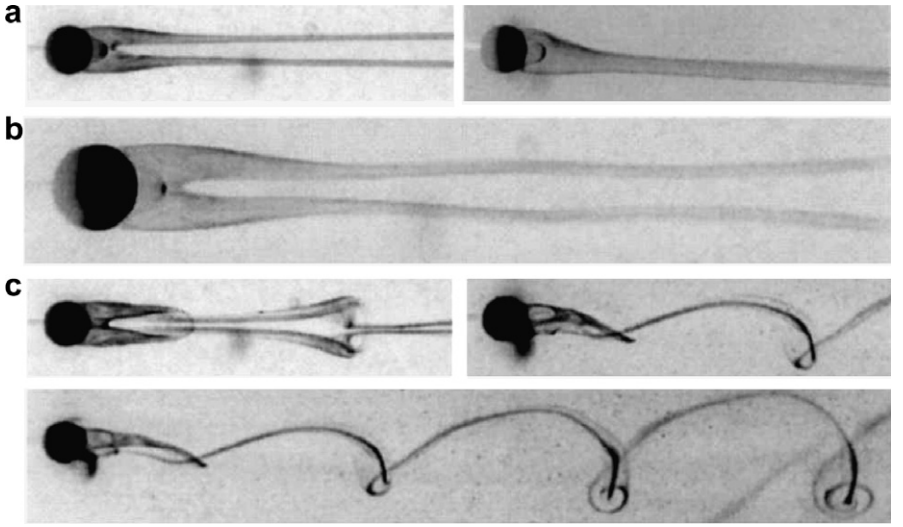

Fig. 1. Visualizations by Schouveiler and Provansal (2002) of the wake behind a sphere held fixed in a uniform stream; (a) $Re \approx 270$, (b) $Re \approx 300$, (c) $Re \approx 345$. (Reprinted from the Physics of Fluids.)

found that consists of two steady counter-rotating threads. At $Re \approx 280$ there is a further transition and the planar-symmetric flow becomes time-dependent: oscillatory patterns appear on the opposite-signed streamwise vortices; for $Re \approx 345$ a series of loops is formed that resemble hairpin vortices. As the Reynolds number is increased further, the flow gradually becomes more irregular and finally turbulent.

A related flow problem of practical importance, namely that of instability and transition of the flow around solid spheres falling or ascending freely in an infinite fluid, has recently been analyzed by Jenny et al. (2003, 2004) (will be referred to as JDB hereafter). The problem is characterized by two non-dimensional parameters, namely ρ_s/ρ, the ratio of the density of the solid sphere, ρ_s, to that of the surrounding fluid, ρ, and the Galileo number G, defined as

$$G = \frac{\sqrt{|\rho_s/\rho - 1| g d^3}}{\nu}. \tag{1}$$

Here d denotes the sphere diameter, ν is the kinematic viscosity of the fluid, and g is the gravitational acceleration. The two parameters G and ρ_s/ρ together define a parameter space. The numerical simulations of JDB show that the spheres, after having been released from rest, reach different 'asymptotic states': their trajectories eventually will have special characteristics that are typical of certain regions of the $(G,\rho_s/\rho)$ parameter space. A diagram indicating these 'regimes' is figure 29 of JDB, which is reproduced here in Fig. 2. Although Section 3.2 of JBD presents some 'preliminary experimental observations' of the motion of the spheres, and although numerous flow visualization studies of the wakes of falling spheres have already been published – the beautiful photographs of Magarvey and Bishop (1961a,b) and Magarvey and MacLatchy (1965) should be noted especially – it seems that an experimental verification of the results found by Dušek's group has not yet been given. Our paper aims at providing such a verification.

JDB's description of the characteristics of the regimes of motion may be summarized as follows: For values of G less than about 156 the spheres fall or ascend along a straight, vertical path due to the axisymmetric flow around the spheres. The axisymmetric flow becomes unstable at a value of G which weakly depends on the value of the density ratio ρ_s/ρ. For example, Jenny et al. (2003) give critical values of $G = 155.8$ for massless spheres, $G = 156.1$ for $\rho_s/\rho = 0.5$, and $G = 159.3$ for spheres that are inhibited to move in a horizontal plane (which effectively means that the mass of the spheres is infinite). At higher values than this first critical value of G, i.e., for parameter values pertaining to the regime indicated by + in Fig. 2 the spheres move at a constant speed along a straight, oblique path; in others words, in a direction not perpendicular to the horizontal plane. The flow around the spheres is steady, but now only planar-symmetric.

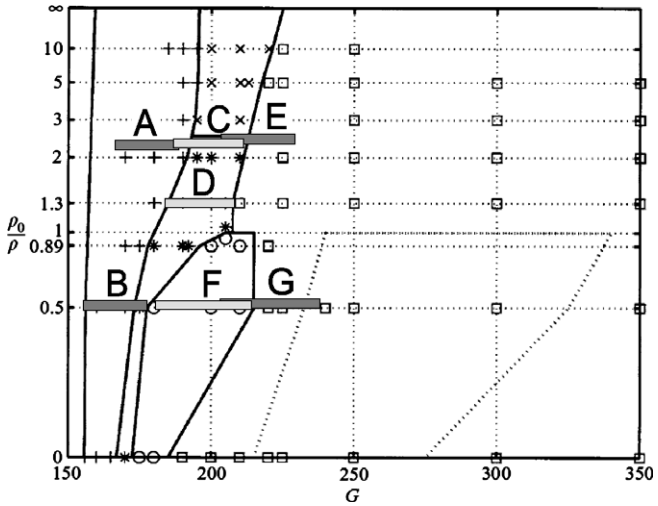

Fig. 2. The different regimes of sphere trajectories in $(G, \rho_s/\rho)$-parameter space, as identified by Jenny et al. (2004): +, steady oblique; ∗, oblique with periodic fluctuations of low-frequency; ×, oblique with periodic fluctuations of high-frequency; ○, zigzag; □, chaotic, with the domain of chaotic and zigzag motion delimited by the dotted line. The rectangular boxes indicate the investigated regions of the $(G, \rho_s/\rho)$-parameter space, where the size of the boxes corresponds to the estimated uncertainty in the values of G and ρ_s/ρ. Information on the values of the physical parameters and the dimensionless numbers is given in Table 1.

At a second critical value of G, which depends much more strongly on the value of ρ_s/ρ, a waviness of the wakes behind the spheres sets in. For parameter values within the regions indicated in Fig. 2 by × and ∗, the spheres follow a path that in the mean is straight and oblique, but involves small periodic excursions in a fixed plane through this oblique path. It appears that two dimensionless frequencies f, defined as

$$f = \frac{f'}{\sqrt{|\rho_s/\rho - 1|g/d}}, \tag{2}$$

with f' the frequency in Hz, may be associated with these excursions: a 'high'-frequency $f \approx 0.180$ in regime × and a 'low'-frequency $0.045 \leqslant f \leqslant 0.068$ in regime ∗; the borderline between the two regimes is the density ratio $\rho_s/\rho \approx 2.5$.

In addition, light spheres (i.e., those with $\rho_s/\rho < 0.5$) only sustain this 'oblique and oscillating regime' over a narrow range of Galileo numbers; beyond a value of G of approximately 175 the spheres ascend along a zigzag path. A characteristic fundamental frequency $0.023 \leqslant f \leqslant 0.035$ is obtained, while a strong third harmonic is also present. This 'zigzagging periodic regime' is indicated in Fig. 2 by ○. The figure also shows that for $\rho_s/\rho > 0.5$ the oblique and oscillating regime extends to larger values of G and, interestingly, that the zigzagging periodic motion is *not* observed for spheres with densities larger than that of the surrounding fluid $(\rho_s/\rho > 1.0)$.

Finally, in the regime indicated by □ the sphere trajectories are 'chaotic'. For spheres with a density higher than that of the surrounding fluid this means that superposed on the seemingly smooth trajectories are small random excursions, without any apparent dominant frequency. This may be contrasted with the chaotic motion of spheres with a density less than that of the fluid, which is characterized by high-velocity fluctuations for which the Fourier transforms of the horizontal components show a definite peak at $f \approx 0.14$. In addition, the wandering motion may be interrupted by periods in which the spheres are zigzagging regularly at a much lower frequency; JDB give an example (see their figure 25) in which this 'low'-frequency $f \approx 0.038$, i.e., comparable to the characteristic frequencies of the zigzagging periodic regime (○). JDB also point at the possibility that for $\rho_s/\rho < 1$ there is a special subdomain of the chaotic regime: in the region delimited by the dotted line in Fig. 2 special initial conditions (cf. JDB's figures 26, 27 and 28) may result also in a periodic zigzagging motion; but now the characteristic frequency is the above-mentioned 'high'-value $f \approx 0.14$.

After a brief description in Section 2 of the materials and methods used, we present in Section 3 an overview of the sphere trajectories that were observed in the experiments. The values of the dimensionless parameters

ρ_s/ρ and G cover most of the regimes described here. A puzzling result of the numerical simulations by JDB is the absence of a 'bifid wake' (a wake consisting of two counter-rotating vortices) behind the spheres. Flow visualization studies by Magarvey and Bishop (1961a,b), Magarvey and MacLatchy (1965) and, more recently, by our group (Veldhuis et al., 2005), have revealed the presence of such a bifid wake. Some new flow visualizations, which corroborate what was found in the earlier studies, are presented in Section 4. The paper ends with conclusions in Section 5.

2. Materials and methods

The experimental set-up used to study the trajectories of the spheres is a perspex tube with height 250 cm and diameter 16 cm (see Fig. 3). At the bottom or the top (depending on whether the spheres would rise or fall) it is equipped with special devices to introduce the spheres. The falling spheres are released from a clamp after which they decent through a funnel, with a final diameter of 15 mm, in order to position the sphere in the center of the perspex tube. The rising spheres are released from a revolver-like mechanism; a flat circular ground plate (20 mm in height, diameter 15 cm) consisting of holes (diameter 15 mm) all at the same radius of 6 cm positioned on the plate. Every hole is occupied by one sphere. On top of the ground plate a cover plate with one hole can be rotated; so the spheres can be released one by one. After release the spheres rise through an inverted funnel with an end diameter of 15 mm before the sphere reaches the water tank.

The measurement section (at the opposite end) is enclosed by a rectangular tank filled with tap water, to match the refraction index of the perspex and to minimize optical distortions. A halogen lamp behind a diffusive plate illuminates the measurement section. By the use of a mirror a side view is obtained; the front and side view are recorded with a Kodak CR 2000 camera (383×512 pixels) at a frame rate of 500 or 1000 frames/s; image processing then yields the three-dimensional positions of the spheres. The field of view is limited to 15 cm × 15 cm × 38 cm resulting in a resolution of 0.9 mm pixel^{-1}. Since the velocities of the spheres are in the range 20–25 m s^{-1}, frequencies of 222–278 Hz are present in the data due to 'pixel effects'. This corresponds to non-dimensionless frequencies in the range of 4–10, which is well beyond the range identified by JDB.

The density ratio ρ_s/ρ and the Galileo number G were varied by using different fluids, tap water and mixtures of water and glycerine, and by using different spheres. The temperature was set at 20 °C. The selection of results presented in this paper is based on experiments with glass spheres ($d = 2.47 \pm 0.03$ mm, $\rho_s = 2470 \pm 30$ kg m^{-3}), polyamide–imide spheres (Torlon; $d = 3.96 \pm 0.01$ mm, $\rho_s = 1410 \pm 20$ kg m^{-3}), and hollow spheres of high-density poly-ethylene (HDPE; $d = 6.35 \pm 0.01$ mm, $\rho_s = 920 \pm 20$ kg m^{-3}). The mass fraction of glycerine of the fluid ranged between 28% and 51%. The viscosity of the fluids was calculated from this mass fraction using the Handbook of Chemistry and Physics (Weast, 1974). This results in a possible error in the viscosity of less than 3.5%. Further, a Haake RS 600 rheometer was used to verify these calculations. Detailed information on the

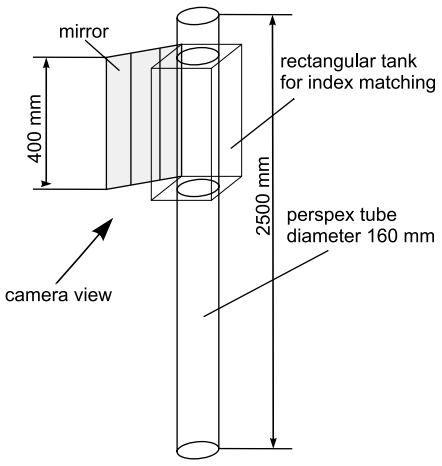

Fig. 3. Sketch of the experimental set-up. The rectangular index matching tank can be moved to the top or bottom of the tank, depending on the type of experiment (falling or rising spheres).

values of the physical parameters and the dimensionless numbers ρ_s/ρ and G is given in Table 1; here the labels A–G refer to the rectangular regions of parameter space indicated in Fig. 2.

In a second experiment the flow behind the spheres was visualized using a Schlieren optics technique (see Fig. 4). The implementation of this technique to study the wakes of gas bubbles was developed by de Vries (2001). Details of the set-up used in the present study are given in Veldhuis et al. (2005), a paper which also includes a large number of Schlieren images of sphere wakes for density ratios close to unity ($0.93 < \rho_s/\rho < 1.05$) and Galileo numbers between 306 and 732, i.e., well within the chaotic regime. The Schlieren technique relies on creating a slight temperature gradient in the fluid, of about 1.0 K cm^{-1}, by heating the fluid from above with infrared light. Fluid of a different temperature (hence different density) is entrained in the wakes of the spheres, and these density gradients are visualized by the Schlieren technique. The 'background' temperature gradient induces an additional buoyancy force on the spheres, but this effect may be shown to be negligibly small (de Vries, 2001).

The Schlieren technique limits the size of the tank: here we used a rectangular glass container of 15 cm × 15 cm × 50 cm. The vertical field of view is 9 cm; this is set by the diameter of the lenses just behind and in front of the tank being 10 cm; to eliminate optical distortions we do not use the outer rim (0.5 cm) of these lenses. This field of view yields a resolution of 0.2 mm pixel^{-1}. The conditions were chosen such that in

Table 1
Values of the physical parameters and the dimensionless numbers in the series of experiments A–G, where the capitals A–G correspond to the rectangular regions within parameter space indicated in Fig. 2

	Material	d (mm)	ρ_s (kg m^{-3})	%	ν (10^{-6} m^2 s^{-1})	ρ_s/ρ	G
A	Glass	2.47	2470	31.0	2.54	2.31 ± 0.05	176 ± 11
B	HDPE	6.35	630	51.0	6.34	0.56 ± 0.03	166 ± 15
C	Glass	2.47	2470	28.0	2.27	2.32 ± 0.05	198 ± 12
D	Torlon	3.96	1410	28.0	2.27	1.32 ± 0.04	195 ± 13
E	Glass	2.47	2470	26.0	2.13	2.33 ± 0.05	212 ± 13
F	HDPE	6.35	630	47.5	5.28	0.56 ± 0.03	198 ± 17
G	HDPE	6.35	630	45.5	4.80	0.57 ± 0.03	218 ± 19

Given are the material of the spheres (HDPE: high-density poly-ethylene; Torlon: polyamide–imide), their diameter d and density ρ_s, the mass percentage of glycerine (%) of the mixtures and their kinematic viscosity ν, the density ratio ρ_s/ρ and the Galileo number G as defined in Eq. (1). The last two columns include estimates of the uncertainty of the given values.

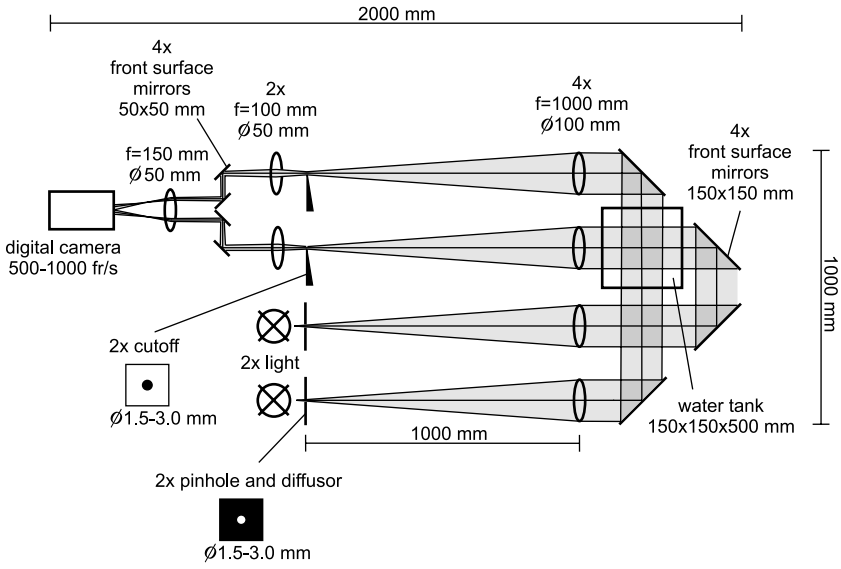

Fig. 4. Schematic top view of the stereoscopic Schlieren set-up. Grey areas indicate the light bundles, f the focal distance of the lenses and ϕ the diameter.

the center of the field of view the fluid properties have the values given in Table 1. The visualizations of the wakes behind the spheres discussed in Section 4 concern the regions of parameter space labeled B, C and F in Fig. 2; however, the spheres may not yet have reached the 'asymptotic state'.

3. The motion of the spheres

We will now discuss the various paths along which the spheres were observed to rise up or fall down the long perspex tube. It is convenient to do this using views from above, which were reconstructed from the stereoscopic recordings made from the sides. For each of the cases A–G, a series of paths will be shown (the left column of Figs. 5, 6 and 8). In every individual case each path corresponds to one experiment with a different sphere, but with the same values for the density ratio and Galileo number. Each path has been given a number to simplify the discussion and the circle indicates the wall of the perspex tube. The frame of reference is centered with its Z-axis on the centerline of the tube and with $Z = 0$ at the position of release of the spheres. The positive Z-axis points upwards for arising sphere and downwards for a falling sphere. Next to the views from above a 'three-dimensional reconstruction' of one of the paths is shown (the right column of Figs. 5, 6 and 8), thus providing an example that represents well the regime identified by JDB.

3.1. Steady and oblique regime: Cases A and B

JDB find that for Galileo numbers a little higher than the critical value for the primary instability, the spheres move steadily along a straight non-vertical path. Although there are a few exceptions, the majority

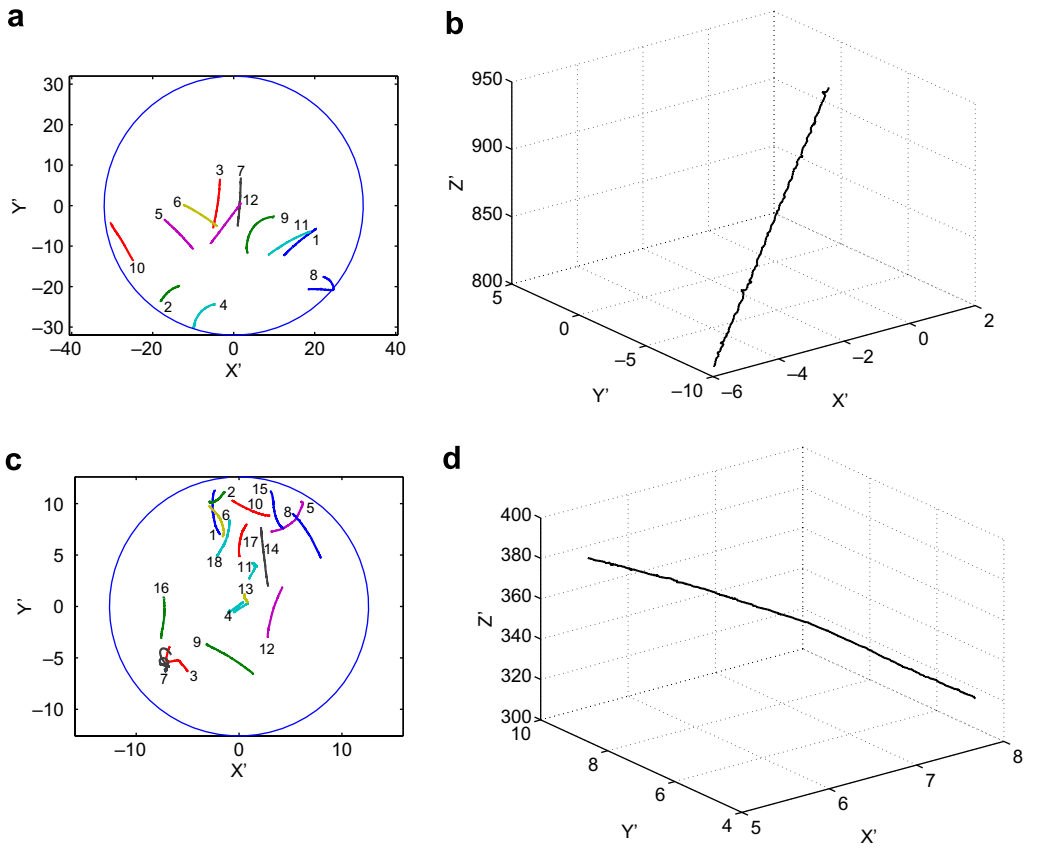

Fig. 5. Left column: Top views of observed particle trajectories in the steady and oblique regime; (a) case A, (c) case B. Right column: 3D reconstruction of one of the paths shown on the left; (b) experiment 12, (d) experiment 8. Distances have been non-dimensionalized by the diameters of the spheres. (For interpretation of the figure in colour, the reader is referred to the web version of this article.)

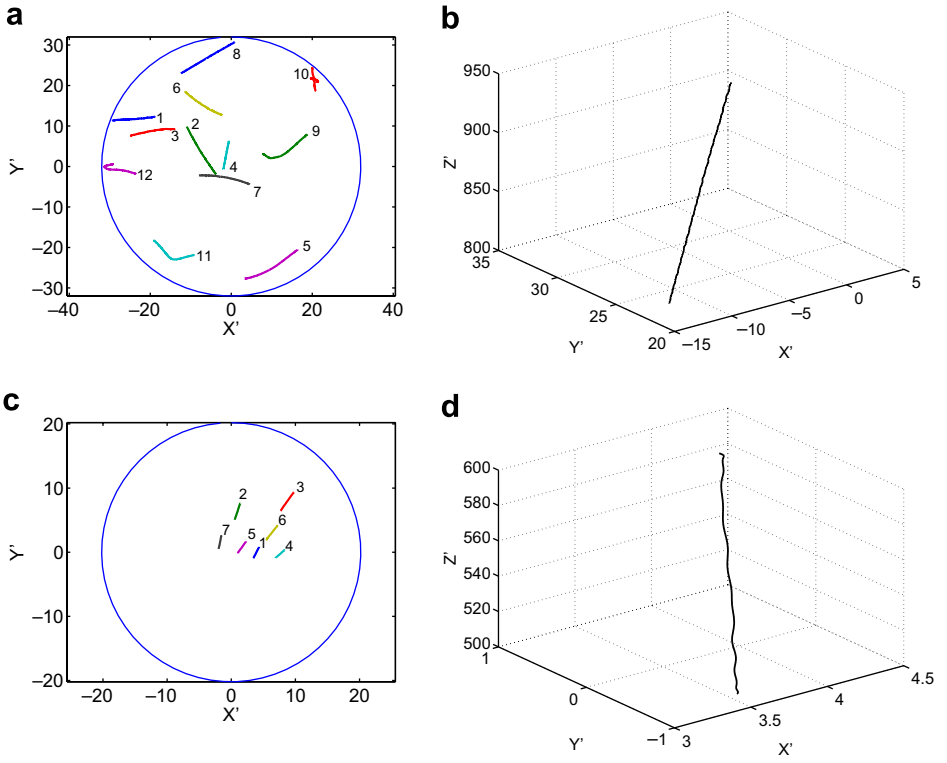

Fig. 6. Left column: Top views of observed particle trajectories in the oblique and oscillating regime; (a) case C, (c) case D. Right column: 3D reconstruction of one of the paths shown on the left; (b) experiment 8, (d) experiment 1. Distances have been non-dimensionalized by the diameters of the spheres. (For interpretation of the figure in colour, the reader is referred to the web version of this article.)

of the paths of the falling glass spheres shown in Fig. 5a, case A, is consistent with the predictions of JDB. The curvature of the paths found in experiments 2, 4, and 9 may be due to a slight non-sphericity of the particles or, in experiments 2 and 4, due to interactions with the wall. The sudden change of direction in experiment 8 indicates that the sphere has hit the wall of the tank.

Most of the paths shown in Fig. 5c, case B, are slightly curved, but not to the extent that JDB's prediction must be considered as incorrect. In these experiments hollow high-density poly-amide (HDPA) spheres were used, and a density distribution that is not perfectly spherically symmetric may be the reason that the paths are not straight. We have no explanation for the somewhat wiggly paths found in experiments 4 and 7. It may be noted that there is a resemblance with the paths found in the experiments of case F, see Fig. 8c. Hollow HDPA spheres were also used in that case, but with slightly larger diameter. Fig. 2 shows that the edge of region B is close to that of region F; due to the uncertainties, experiments 4 and 7 may have been conducted at the outer border of regime B.

The existence of the steady oblique regime, which even includes solid spheres of negligible mass, may be a little surprising for those who are more familiar with the behavior of gas bubbles. The primary instability of the flow around gas bubbles eventually leads to a zigzagging or spiralling motion (something that was known already to Leonardo da Vinci; cf. Prosperetti, 2004). That this is not what is observed for massless solid spheres suggests that the very different behavior of gas bubbles is due to their ability to deform easily.

3.2. Oblique and oscillating regime: Cases C and D

In the experiments of case C the same glass spheres were used as in the experiments of case A, but the fluid properties where adjusted – this changes the value of G, but hardly affects the value of ρ_s/ρ – so that the parameter values would correspond to what JDB specify as the periodic oblique regime. In fact, the value

2.32 of the density ratio ρ_s/ρ in case C is just below 2.5, which JBD estimate as the value which divides the periodic oblique regime into two parts: one with high-frequency velocity fluctuations ($\rho_s/\rho > 2.5$) and another with low-frequency velocity fluctuations ($\rho_s/\rho < 2.5$). The experiments of case D should correspond to the low-frequency periodic oblique regime and were conducted with polyamide–imide (Torlon) spheres.

For case C, most of trajectories shown in Fig. 6a are oblique and deviate little from a straight line. Exceptions are the experiments 10 and 12 in which the strong curvature of the path is due to collisions with the wall. While a Fourier analysis of the components of the horizontal velocity fluctuations in cases A and B does not yield anything significant, a similar analysis of case C shows dominant non-dimensional frequencies f of approximately 0.07 and 0.25, while there is also evidence of the presence of a non-dimensional frequency of approximately 0.17 (see Fig. 7a). The first frequency is close to the range $0.045 \leqslant f \leqslant 0.068$ mentioned by JDB as typical of the low-frequency oblique and oscillating regime, while the second frequency corresponds to a higher (third or fourth) harmonic. The small peak at 0.17 seems to agree with the value $f \approx 0.18$, which according to JDB characterizes the high-frequency oblique and oscillating regime. This suggests that there is a region of parameter space in which there is smooth transition between the two regions that constitute the oblique and oscillating regime identified by JDB.

The trajectories observed for case D, with the polyamide–imide spheres, are presented in Fig. 6c. Ignoring the minor deviations, these are indeed perfectly straight oblique paths. Fourier analysis of one of the horizontal velocity components in experiment 1 reveals (see Fig. 7b) again a dominant non-dimensional frequency f of approximately 0.25. In some of the spectra broad, but much smaller, peaks may be observed at frequencies between 0.06 and 0.14 (as in Fig. 7b). Thus, a 'fundamental frequency' in the range identified by JDB, $0.045 \leqslant f \leqslant 0.068$, is usually present, but that a higher (fourth) harmonic always dominates.

3.3. Zigzagging periodic regime and chaotic regime: Cases E, F, and G

In the experiments of case E the same glass spheres were used as in the experiments of cases A and C. By adjusting the fluid properties, a region of parameter space was selected which according to JDB should lie at the border, but just within, the chaotic regime. Some of the observed trajectories are shown in Fig. 8a. They differ from the trajectories of case C (the oblique and oscillating regime) shown in Fig. 6a by having much stronger variations in curvature. There is a clear resemblance with the trajectory shown in figure 20 of JDB, calculated for $\rho_s/\rho = 5$ and $G = 250$; though the limited field of view made it impossible to detect the slow helicoidal motion visible in that figure. Fourier analysis of the components of the projection of the velocity vector did not reveal the presence of any dominant frequencies, and qualifying this regime of parameter space as chaotic seems to be justified.

The trajectories found in the experiments of cases F and G are shown in Fig. 8c and e. According to JDB's classification, case F belongs to the zigzagging periodic regime and case G to the chaotic regime. Despite this, the trajectories have a similar appearance: in both cases a zigzagging is found occasionally, but more often the spheres follow an irregular zigzag path. These experiments were conducted with hollow HDPE spheres, and, as was argued above, the density distributions of many of these may not have been perfectly spherically

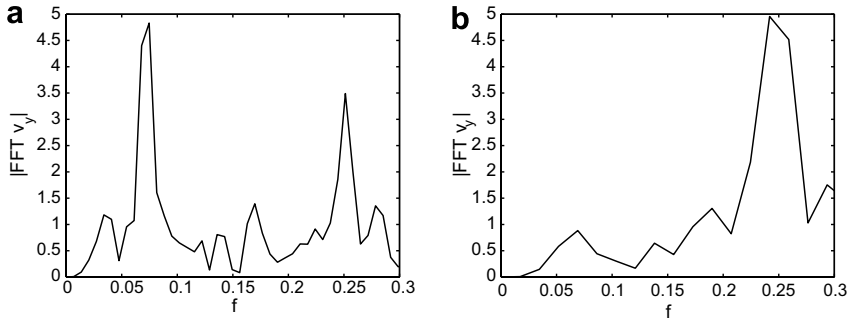

Fig. 7. Fourier transforms of one of the horizontal velocity components in the oblique and oscillating regime, (a) case C, experiment 4; (b) case D, experiment 1. The frequency has been non-dimensionalized as indicated by Eq. (2).

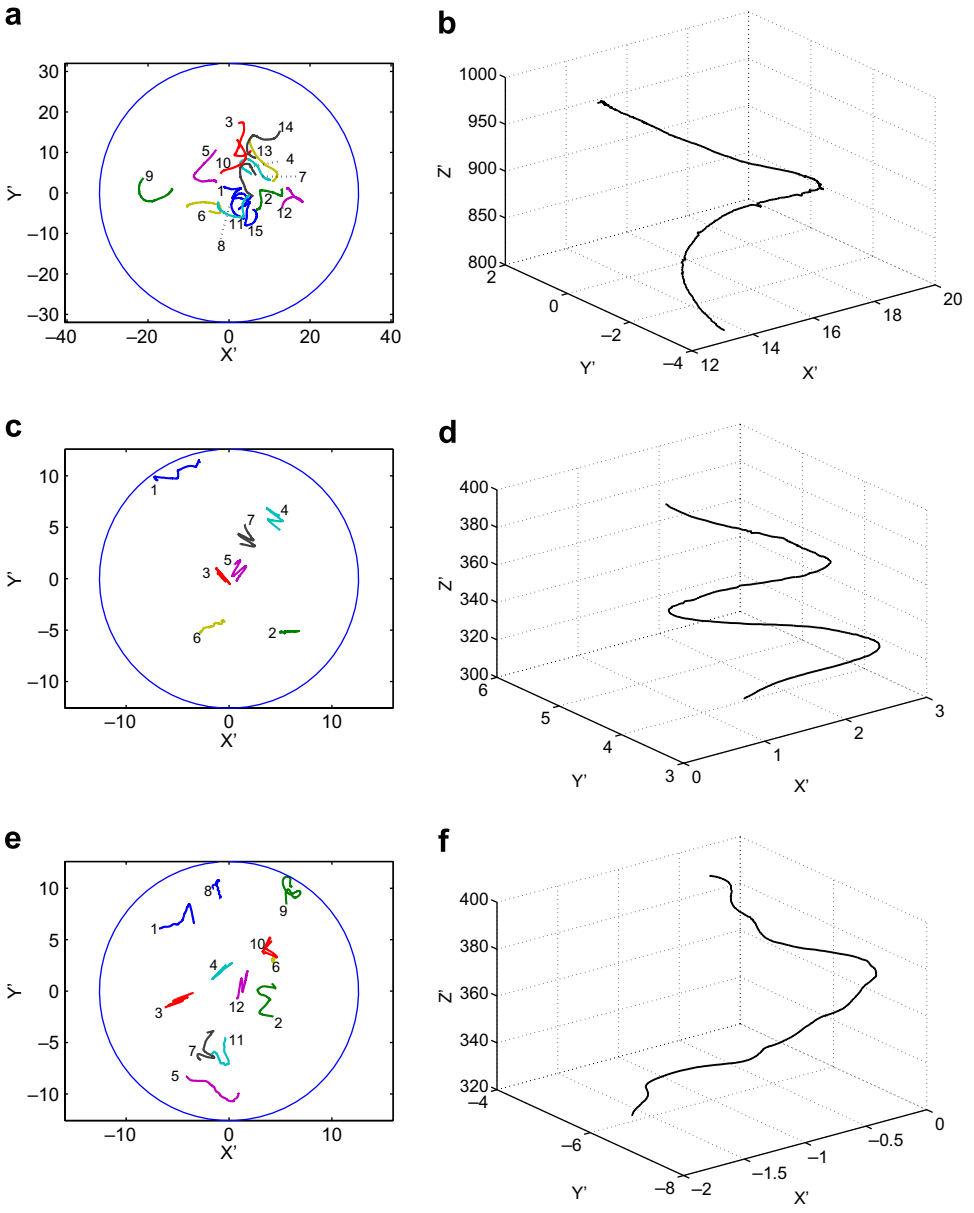

Fig. 8. Left column: Top views of observed particle trajectories in the zigzagging periodic regime and the chaotic regime; (a) case E, (c) case F, (e) case G. Right column: 3D reconstruction of one of the paths shown on the left; (b) experiment 12, (d) experiment 7, (f) experiment 11. Distances have been non-dimensionalized by the diameters of the spheres. (For interpretation of the figure in colour, the reader is referred to the web version of this article.)

symmetric. It seems that the observations of case F agree with the discussion in Section 10 of JDB, where it is argued that slight inhomogeneities are sufficient to destroy the zigzagging periodic regime (cf. also their figure 31). Hence, in both cases F and G the motion of the spheres must be considered as chaotic, the zigzag paths being instances of the special character of the chaotic regime for ascending spheres as identified by JDB (see their figures 25 and 27); namely, that the erratic motion may be interrupted by short periods in which the spheres move along a zigzag.

Further support for these conclusions may be found by considering the Fourier transform of a horizontal velocity component of a zigzagging particle, such as shown in Fig. 9a for experiment 7 of case F, and in Fig. 9b for experiment 3 of case G. Both spectra show a large peak at a dimensionless frequency f of about 0.052.

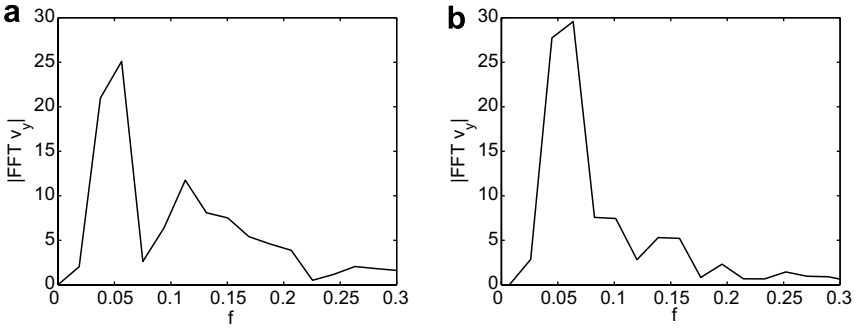

Fig. 9. Fourier transforms of one of the horizontal velocity components, (a) zigzagging periodic regime; case F, experiment 7; (b) chaotic regime; case G, experiment 3. The frequency has been non-dimensionalized as indicated by Eq. (2).

We have no explanation for the appearance of this frequency, but it is certainly much higher than the fundamental frequency of the zigzagging periodic regime, which according to JDB should lie within the range $0.023 \leqslant f \leqslant 0.035$. It may be noted that also a further characteristic of the zigzagging periodic regime, i.e., a strong third harmonic, is absent from Fig. 9a. Instead, broad peaks are observed at dimensionless frequencies of approximately 0.12 in Fig. 9a and 0.14 in Fig. 9b, values that agree very well with the value of $f = 0.14$ mentioned by JDB as characteristic of the 'zigzagging spots' within the chaotic trajectories.

To conclude this section, it may be noted that, on comparing Fig. 8a with Fig. 8c and e, the behavior of the light, ascending, HDPE spheres differs considerably from that of the heavy, falling, glass spheres. This supports the conclusions of Karamanev and Nikolov (1992) and Karamanev et al. (1996); namely, that the motion of 'light' spheres (which they associate with a density ratio $\rho_s/\rho < 0.3$) is truly different from that of heavy spheres; the upshot being that the standard drag correlation $C_D(Re)$, with the Reynolds number Re and the drag coefficient C_D based on the mean vertical velocity, does not apply for these light spheres. The motion of rising light solid spheres at high-values of G has recently been studied by Veldhuis et al. (submitted for publication).

4. The wakes of the spheres

It was already mentioned that for values of G slightly higher than that for which the axially symmetric flow around a gas bubble rising in clean water becomes unstable, the bubble will follow a zigzag or helicoidal path.

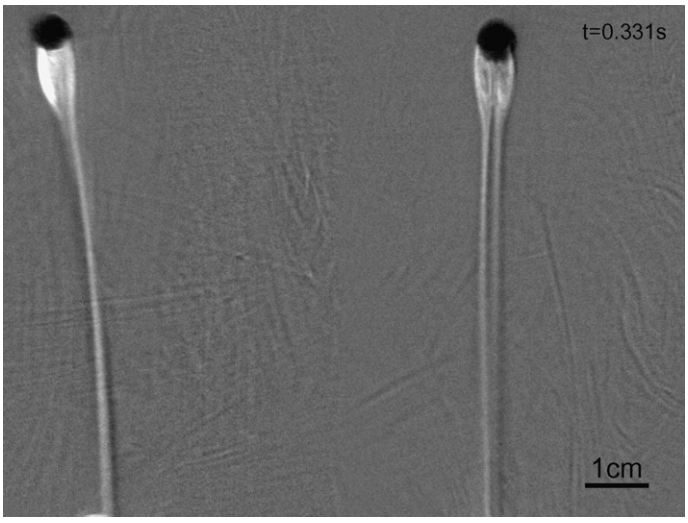

Fig. 10. Stereoscopic Schlieren image of the wake of a rising sphere in the steady and oblique regime (case B). The picture was taken $t = 0.331$ s after the sphere had entered completely the field of view.

The wake of such a bubble consists of two counter-rotating vortices, as was established by the numerical work of Mougin and Magnaudet (2002) and the flow visualizations of de Vries et al. (2002). This behavior is quite different, as shown first by JDB and confirmed by our study, from that of solid spheres, which in the analogous situation rise or fall along a straight non-vertical path. JDB also find that the wakes behind these particles do not have a bifid structure. Fig. 10 shows a stereoscopic Schlieren image of the wake of a falling sphere in the steady and oblique regime (case B). Obviously, what is visualized here are variations of the density gradient in the fluid, and not the vorticity distribution in the flow. Yet, the picture suggests that the wake consists of two counter-rotating vortices, just like the wakes of zigzagging or spiralling bubbles and the wakes of solid spheres held fixed in a uniform flow (cf. Johnson and Patel, 1999; Schouveiler and Provansal, 2002). The picture seems to disagree with the findings of JDB.

A stereoscopic Schlieren image of the wake of a falling solid sphere in the oblique and oscillating regime (case C) is shown in Fig. 11a. Here the path followed by the sphere between the moment that it entered completely the field of view and the moment that the picture was taken is visualized by the dash–dotted line. The picture shows that an oscillatory wake structure has evolved by a 'self-induced' redistribution of the vorticity.

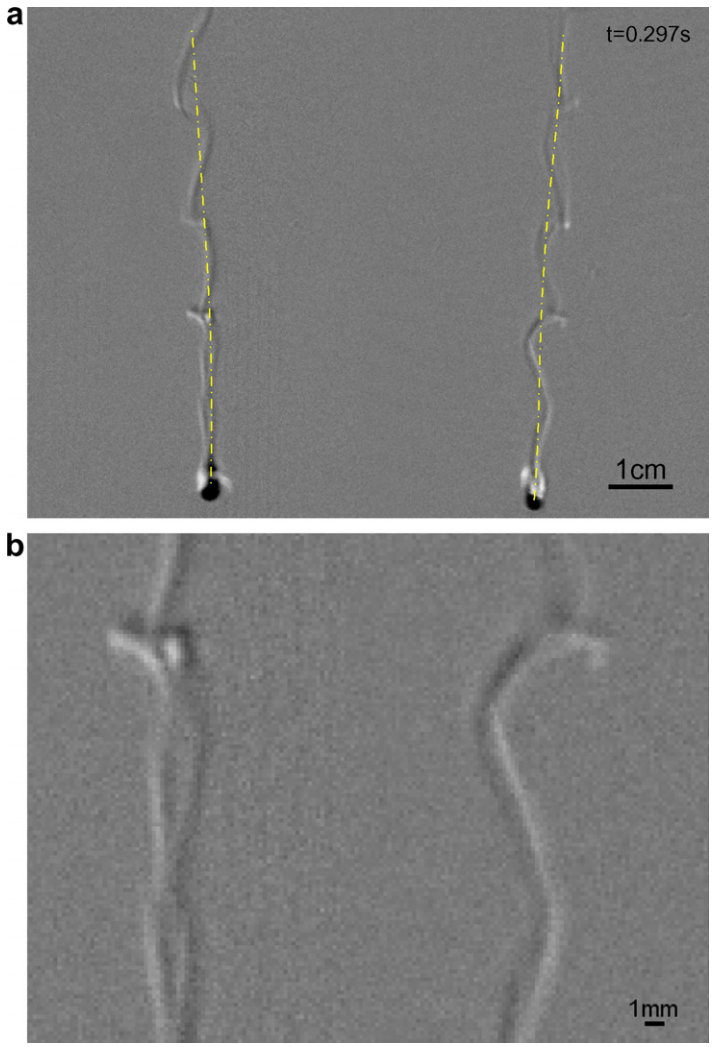

Fig. 11. (a) Stereoscopic Schlieren image of the wake of a falling sphere in the oblique and oscillating regime (case C). The dash–dotted line indicates the path followed by the sphere after it completely entered the field of view $t = 0.297$ s earlier; this is also the starting point of the line. (b) Enlarged view of a detail of (a).

The enlarged view of the wake just behind the sphere, Fig. 11b, supports the description of this process, as given earlier by Veldhuis et al. (2005) (see also their figure3): the two counter-rotating vortices kink, through which they locally get close together (see the region just below the center of Fig. 11b), and subsequently the

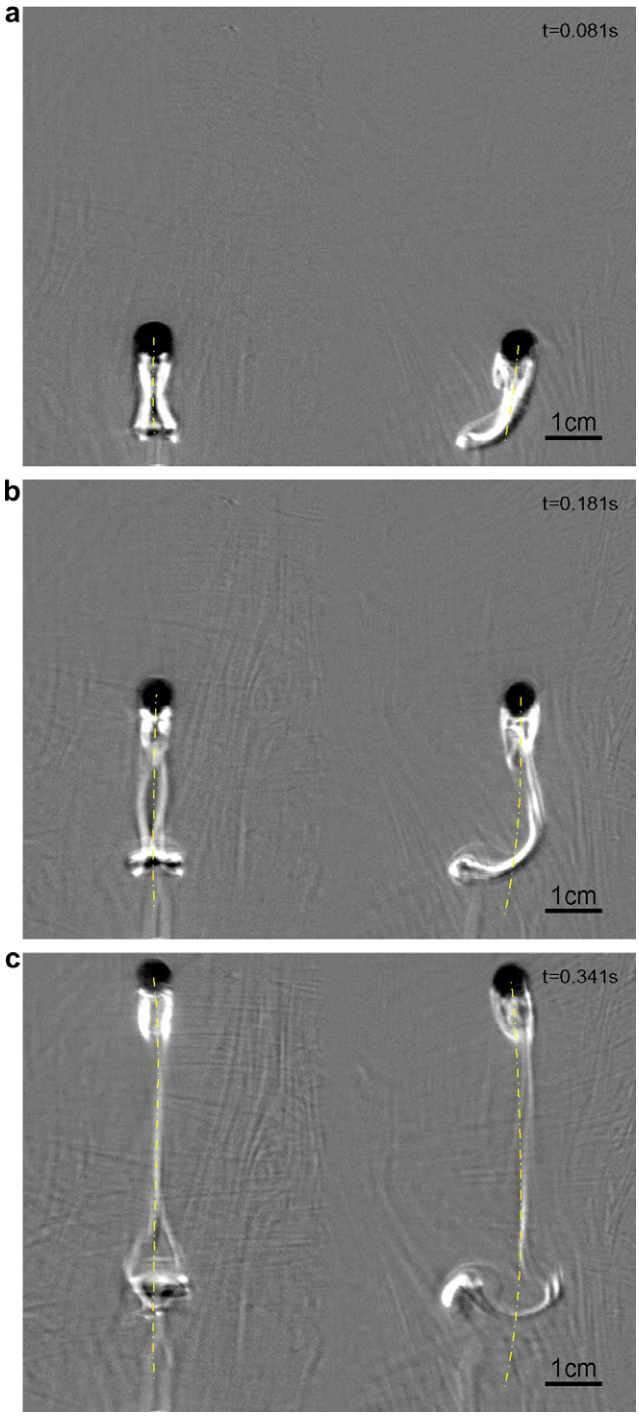

Fig. 12. Schlieren images of the wake of a rising sphere in the 'destroyed' zigzagging periodic regime (case F), showing how the double-threaded wake evolves into a hairpin-like vortex structure. The pictures were taken t seconds after the sphere had entered completely the field of view, (a) $t = 0.081$ s, (b) $t = 0.181$ s, (c) $t = 0.341$ s.

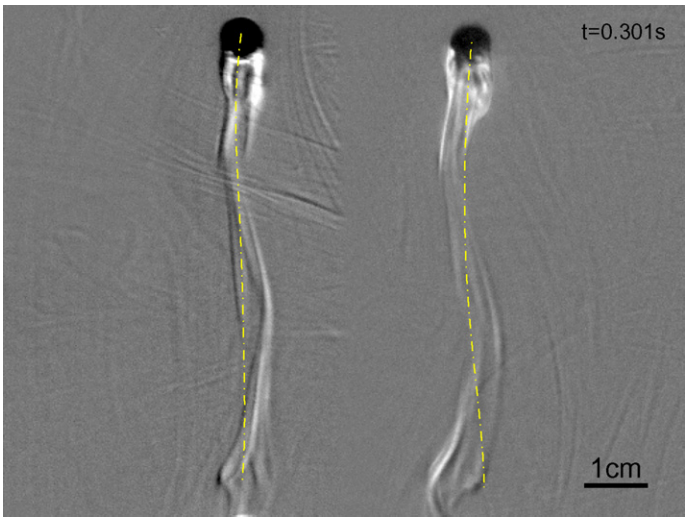

Fig. 13. Stereoscopic Schlieren image of the wake of a rising sphere in the 'destroyed' zigzagging periodic regime (case F). The picture was taken $t = 0.301$ s after the sphere had entered completely the field of view. Note the different character of the wake as compared to that shown in Fig. 12.

two threads of vorticity bend and connect (see the structure near the top of the figure). The smooth sphere trajectory of Fig. 11a also suggests that this process of redistribution of wake vorticity hardly affects the 'overall' motion of the spheres. Yet, it may lead to small fluctuations in the velocity. This becomes evident by associating a 'frequency' with the pattern observed in Fig. 11a. By analyzing the time dependant data the wake frequency can be extracted. This frequency, made dimensionless in the manner of Eq. (2), is estimated as 0.19; a value which indeed coincides with one of the peaks in the Fourier spectrum of a horizontal velocity component, such as shown in Fig. 7a. Note that a rough estimate of the wake frequency can be extracted directly from the Schlieren image by counting the number of wake instabilities in the image and divide this by the elapsed time. Of course, this method does not account for any redistribution of the wake in time.

A further illustration of the evolution of the unstable bifid wake is given in the Schlieren visualizations presented in Fig. 12. This concerns a rising solid sphere in what JDB classify as the zigzagging periodic regime (case F), but which here turned out to be chaotic, as a consequence of a lack of spherical symmetry in the density distribution of the hollow HDPE spheres that were used. That the wake of rising spheres in this regime may also have a somewhat different structure is exemplified in Fig. 13. Figs. 12 and 13 confirm what was mentioned earlier; namely, that the overall motion of the spheres is not affected significantly by the redistribution of the vorticity in the flow. Here again, a dimensionless frequency may be associated with the wake patterns: its value is estimated as between 0.11 and 0.15 for the wake shown in Fig. 12, and between 0.15 and 0.19 for that in Fig. 13. For the case of Fig. 12 this values agrees well with the broad peak observed in the velocity spectrum shown in Fig. 9a. Unfortunately, the limited field of view did not allow us to look for other details of the flow, which might explain the high-peak at $f \approx 0.05$ in Fig. 9a.

5. Conclusions

To the best of our knowledge, the work of Dušek and colleagues (JDB) is the first to give a detailed analysis of the instabilities and transitions in the motion of spheres moving freely under the action of gravity. Our experiments do not give information on the mechanisms involved in these instabilities and transitions. However, our observations agree very well with JDB's description of 'the main features' of the motion of the spheres and how these may be associated with various regimes: regions of the $(G, \rho_s/\rho)$ parameter space for which the motion of the spheres have quite distinct characteristics. Discrepancies found in the experiments with hollow high-density poly-ethylene spheres (case B) may presumably be attributed to a lack of spherical symmetry in the density distribution of these spheres. This is supported by the fact that on using these spheres

no evidence could be found for the existence of JDB's zigzagging periodic regime. JDB show that a slight mismatch in the positions of the center of volume and the center of mass of the spheres destroys this regime; the motion of the spheres is then best described as chaotic. This agrees with what was observed in our case F.

We found some small differences with JDB's description of 'the details' of the motion of the spheres. These concern the values given by JDB of the dominant frequencies that may be observed in the spectra of one of the horizontal velocity components. In particular, our experiments suggest that the oblique and oscillating regime (cases C and D), divided by JDB into two sub-regimes, one with a 'low'-characteristic frequency and one with a 'high'-characteristic frequency, also includes a third sub-regime (case C) in which both of these characteristic frequencies are present. We found evidence for the presence of a fundamental 'low'-frequency within the range identified by JDB, but in all spectra a higher (third or fourth) harmonic appeared to be dominant. Furthermore, the observed velocity spectra of ascending spheres in the chaotic regime (cases F and G) show broad peaks at a dimensionless frequency that agrees fairly well with the characteristic frequency mentioned by JDB; yet, both these spectra also have a distinct peak at a much lower frequency ($f \approx 0.05$), a phenomenon not found by JDB.

Finally, our flow visualizations do not corroborate the remarkable assertion of JDB, namely, the absence of a bifid wake behind the spheres. In all our pictures the wake seems to consists, entirely or in part, of two counter-rotating vortices.

Acknowledgements

We wish to thank Marike Aalbers, Martin Bos and Gert-Wim Bruggert for their invaluable assistance with the experiments, and Detlef Lohse for permission to use his laboratory facilities. A.B. gratefully acknowledges the CNRS for providing financial support for a visit to the Laboratoire de Méanique des Fluides et d'Acoustique at the Ecole Centrale de Lyon. This work is part of the research programme of the Stichting voor Fundamenteel Onderzoek der Materie (FOM), which is financially supported by the Nederlandse Organisatie voor Wetenschappelijk Onderzoek (NWO).

References

Ghidersa, B., Dušek, J., 2000. Breaking of axisymmetry and onset of unsteadiness in the wake of a sphere. J. Fluid Mech. 423, 33–69.
Jenny, M., Bouchet, G., Dušek, J., 2003. Nonvertical ascension or fall of a free sphere in a Newtonian fluid. Phys. Fluids 15, L9–L12.
Jenny, M., Dušek, J., Bouchet, G., 2004. Instabilities and transition of a sphere falling or ascending freely in a Newtonian fluid. J. Fluid Mech. 508, 201–239.
Johnson, T.A., Patel, V.C., 1999. Flow past a sphere up to a Reynolds number of 300. J. Fluid Mech. 378, 19–70.
Karamanev, D.G., Nikolov, L.N., 1992. Free rising spheres do not obey Newton's law for free settling. AIChE J. 38, 1843–1846.
Karamanev, D.G., Chavarie, C., Mayer, R.C., 1996. Dynamics of the free rise of a light solid sphere in liquid. AIChE J. 42, 1789–1792.
Kim, I., Pearlstein, A.J., 1990. Stability of the flow past a sphere. J. Fluid Mech. 211, 73–93.
Lee, S., 2000. A numerical study of the unsteady wake behind a sphere in a uniform flow at moderate Reynolds numbers. Comput. Fluids 29, 639–667.
Magarvey, R.H., Bishop, R.L., 1961a. Wakes in liquid–liquid systems. Phys. Fluids 4, 800–805.
Magarvey, R.H., Bishop, R.L., 1961b. Transition ranges for three-dimensional wakes. Can. J. Phys. 39, 1418–1422.
Magarvey, R.H., MacLatchy, C.S., 1965. Vortices in sphere wakes. Can. J. Phys. 43, 1649–1656.
Mougin, G., Magnaudet, J., 2002. Path instability of a rising bubble. Phys. Rev. Lett. 88, 014502.
Natarajan, R., Acrivos, A., 1993. The instability of the steady flow past spheres and disks. J. Fluid Mech. 254, 323–344.
Ormières, D., Provansal, M., 1999. Transition to turbulence in the wake of a sphere. Phys. Rev. Lett. 83, 80–83.
Prosperetti, A., 2004. Bubbles. Phys. Fluids 16, 1852–1865.
Schouveiler, L., Provansal, M., 2002. Self-sustained oscillations in the wake of a sphere. Phys. Fluids 14, 3846–3854.
Tomboulides, A.G., Orzag, S.A., 2000. Numerical investigation of transitional and weak turbulent flow past a sphere. J. Fluid Mech. 416, 45–73.
Veldhuis, C.H.J., Biesheuvel, A., van Wijngaarden, L., 2005. Motion and wake structure of spherical particles. Nonlinearity 18, C1–C8.
Veldhuis, C.H.J., Biesheuvel, A., Lohse, D., submitted for publication. Freely rising light solid spheres. J. Fluid Mech.
de Vries, A.W.G., 2001. Path and Shape of a Rising Bubble. Ph.D. thesis, University of Twente.
de Vries, A.W.G., Biesheuvel, A., van Wijngaarden, L., Lohse, D., 2002. Notes on the path and wake of a gas bubble rising in pure water. Int. J. Multiphase Flow 28, 1823–1835.
Weast, R.C., 1974. Handbook of Chemistry and Physics, 55th ed. CRC Press.